

RESEARCH PAPER

Green synthesis of Ag-NPs as a metal nanoparticle and ZnO-NPs as a metal oxide nanoparticle: Evaluation of the *in vitro* cytotoxicity, anti-oxidant, anti-angiogenic activities

Hoda Shabestarian¹, Masoud Homayouni Tabrizi^{2*}, Monireh Movahedi¹, Ali Neamati², Fariba Sharifnia³

¹Department of Biochemistry, Faculty of Biological Science, North Tehran Branch, Islamic Azad University, Tehran, Iran

²Department of Biology, Mashhad Branch, Islamic Azad University, Mashhad, Iran

³Department of Biology, Faculty of Biological Science, North Tehran Branch, Islamic Azad University, Tehran, Iran

ABSTRACT

Objective(s): The study aimed to synthesize both silver- and zinc-oxide nanoparticles utilizing the Peganum harmala smoke extract (PHSE) bio-platform to evaluate their cytotoxicity on different types of human cancer cell lines and study their anti-oxidant, and anti-angiogenic potentials.

Materials and Methods: The Silver (Ag) and zinc oxide (ZnO) nanoparticles (NP) were produced utilizing the green-synthesize method by applying the PHSE bio-platform. After characterization by X-Ray Diffraction (XRD), dynamic light scattering (DLS), Field emission scanning electron microscopy (FESEM), and Fourier-transform infrared spectroscopy (FTIR) methods. MTT assay was used for the evaluation toxicity of nanoparticles. ABTS, DPPH, FRAP, and ROS for anti-oxidant capacity, chicks' chorioallantoic membrane (CAM), and qPCR for anti-angiogenesis effects of nanoparticles were used.

Results: Ag-NPs (82.42 nm) and ZnO-NPs (163.05 nm) inhibited prostate, ovarian, and liver malignant cells. Inhibition of ABTS•+ and DPPH•+ and increasing the rate of intracellular ROS exhibited the anti and pro-oxidant capacity of Ag and ZnO-NPs out and inside of malignant cells. Also, their anti-angiogenesis impact was verified by significant dose-dependent VEGF and VEGFR down-regulation and the decreased blood vessels in the CAM.

Conclusion: The anti-oxidant, cytotoxicity and anti-angiogenesis effects of Ag and ZnO-NPs synthesized from Pecan smoke extract make it possible to use these nanoparticles in cancer chemotherapy.

Keywords: Angiogenesis inhibitors, Anti-oxidants, Metal nanoparticles

How to cite this article

Shabestarian H, Homayouni Tabrizi M, Movahedi M, Neamati A, Sharifnia F. Green synthesis of Ag-NPs as a metal nanoparticle and ZnO-NPs as a metal oxide nanoparticle: Evaluation of the *in vitro* cytotoxicity, anti-oxidant, anti-angiogenic activities. *Nanomed J.* 2023; 10(3): 245-258. DOI: 10.22038/NMJ.2023.71700.1770

INTRODUCTION

Nanotechnology is one of the emerging branches of science with wide application in the field of biomedicine [1]. Size-dependent quantum effects alter the physicochemical and biological properties of nanomaterials relative to their bulk counterparts. The small size of nanoparticles and the presence of a higher percentage of atoms on their surface make it possible to interact with biomolecules both on the surface and inside

the cells of the body and can lead to achieving methods for diagnosing and treating cancer [2].

Nanotechnology has taken an important step in improving the quality of anti-cancer drugs by producing nano drugs and targeting tumor cells [3]. One of the important fields of study in biomedical sciences is the evaluation of the pharmacological properties of nanomaterials [4]. Silver (Ag) and zinc oxide (ZnO) nanoparticles Due to their unique physical and chemical properties, ZnO-NPs are one of the most important metal oxide nanoparticles. In personal care products, such as cosmetics and sunscreen, ZnO is increasingly used due to its strong UV absorption properties [5]. Furthermore, ZnO nanoparticles possess superior

* Corresponding author: Email: mhomayouni6@gmail.com; mhomayouni6@mshdiau.ac.ir

Note. This manuscript was submitted on March 10, 2023; approved on May 14, 2023

antibacterial, antimicrobial, and UV-blocking properties. Consequently, in the textile industry, the finished fabrics containing ZnO NPs exhibit the desirable features of being ultraviolet and visible light resistant, antimicrobial, and deodorizing [6, 7]. These properties have led to increased interest in ZnO nanoparticles in biomedical applications. The relatively low cost and relatively less toxic properties of ZnO nanoparticles make them particularly suitable for biomedical applications, including anticancer, drug delivery, antibacterial, diabetes treatment, antiinflammation, wound healing, and bioimaging [8, 9]. Biomaterials based on nanosilver were tested against a variety of pathogenic microorganisms, including bacteria, viruses, fungi, and yeasts [10]. In addition to their impressive antimicrobial properties, silver nanoparticles represent an effective starting point for the development of new and performance-enhanced biomedical products based on silver such as anticancer agents, drug-delivery platforms, orthopedic materials, and devices. Because of the impressive applications of AgNPs in nanotechnology, biomedicine, and the environment, cost-effective methods for synthesis of AgNPs are constantly in demand [11, 12]. Ag-NPs and ZnO-NPs have recently attracted considerable attention due to their beneficial and potential effects on human health [13]. The use of plant extracts and natural products as reducing and stabilizing agents in the synthesis of these nanoparticles (green synthesis) can increase clinical efficiency and reduce the effects of toxicity and inefficiency of nanoparticles synthesized by chemical and physical methods [14]. In various studies, the anti-oxidant [15, 16], anti-cancer [17, 18], antimicrobial [19, 20], and anti-angiogenesis [21, 22] activities of these nanoparticles have been investigated and confirmed.

NPs can lead to cell death by increasing the intracellular reactive oxygen species (ROS), followed by increased oxidative stress and inflammatory products such as cytokines [6, 23]. ROS are produced as byproducts of oxygen metabolism in the body and play several physiological roles, such as cellular signaling. However, some factors such as environmental stressors help increase ROS production and subsequently cause an imbalance in production and its elimination by the anti-oxidant system. Anti-oxidants play an important role in the body's defense against the damaging effects of free radicals and ROS. An imbalance

between anti-oxidants and ROS causes oxidative stress and subsequent cell damage [24]. Although an increase in ROS in healthy cells can cause carcinogenesis, however, the increase in ROS and subsequent damage to biological macromolecules and the initiation of apoptosis is one of the most important mechanisms for the removal of cancer cells in chemotherapy [25]. Despite the inhibitory effect of ZnO and Ag nanoparticles on free radicals in vitro [15, 16], their role in the production of oxidative stress following the increase in ROS in cancer cells has been shown in various studies [26, 27]. Cancer cells have a negative charge on their surface due to the high percentage of anionic phospholipids and certain groups of charged proteins and carbohydrates on their surface, and this feature can cause electrostatic interaction of nanoparticles with a positive surface charge to cancer cells as target cells [28, 29]. Exposure of cancer cells to nanoparticles activates cellular defense mechanisms to minimize damage, and if the stimulation of ROS production within the cell by nanoparticles is greater than the cell's anti-oxidant defense capacity, the cells undergo apoptosis [6, 23]. Other effective mechanisms of nanoparticles in inhibiting cancer cells include inhibition of angiogenesis and their anti-cancer effects. Studies have shown that cells in tumor tissue create new blood vessels, by secreting stimulatory factors. Therefore, the initial growth of the tumor and its continued growth depends on the adequate blood supply to the tumor tissue, and inhibition of blood flow can prevent further tumor growth [30]. Various studies have confirmed the inhibitory effect of silver [22] and ZnO-NPs [21] on angiogenesis. However, some studies have reported the pro-angiogenesis effects of ZnO-NPs [31].

Researchers have recently begun to explore the potential for using plant flavonoids, terpenoids, and alkaloids to formulate anticancer agents. The medicinal plant Harmal, *Peganum harmala* L, is a member of the Zygophyllaceae family and is widely distributed in Central Asia, North Africa, and the Middle East [32]. Traditional medicine has long used the seeds, fruits, roots, and bark of this plant. The chemical composition of this plant has been studied, and it has been shown that it contains beta-carboline, quinazoline, harmaline, and harmine alkaloids. These compounds are responsible for their beneficial effects, including hypnotic, anticancer, antiperspirant, antibacterial,

antifungal, and anti-inflammatory properties [33]. Furthermore, some studies have reported that smoke from the seeds of this plant is anti-cancer and anti-bacterial in addition to its medicinal effects. Smoke collected from pecans is dissolved in N-hexane and exhibits hydrophobic properties. The use of nanocarriers allows active compounds to be solubilized and more readily absorbed by cancer cells, eliminating the limitations of their solubility and bioavailability [34].

The aim of this study was to use pecan smoke extract was to synthesize ZnO-NPs and Ag-NPs through green method. After characterization of the nanoparticles, their anti-oxidant, cytotoxicity properties, and anti-angiogenesis effects of ZnO-Ag nanocomposites were investigated *in vitro*.

MATERIALS AND METHODS

Materials

2,2'-azino-bis(3-ethylbenzothiazoline-6-sulfonic acid) (ABTS), 2,2-diphenyl-1-picrylhydrazyl (DPPH), 3-(4,5-dimethylthiazol-2-yl)-2,5-diphenyltetrazolium bromide (MTT), ferric tripyridyl triazine (Fe^{3+} TPTZ), Dimethyl sulfoxide (DMSO), Zinc acetate, and silver nitrate were purchased from Merck Co. The human cancer cell lines including human prostate cancer (PC3), ovarian cancer (A2780), human liver cancer (HepG2) cell lines, and human foreskin fibroblast (HFF) non-cancerous normal cells were purchased from Ferdowsi University of Mashhad, Iran. All the materials needed for cell culture were bought from Sigma Aldrich.

Peganum harmala seeds (PHS) extraction

The dried *Peganum harmala* seeds (1000 g) were burned at 80 °C in a 1000-mL distilling flask. The oxygen gas was injected 1 puff per 5 min during burning. Then, the smoke components were collected by cooling and distilling them in a condenser tube. N-Hexane was used as the collector solvent then, the *Peganum harmala* smoke extract (PHSE) was dried.

Zn-oxide nanoparticles synthesis

Zinc acetate (9 g) was added in 20 mL distilled water (DW) and mixed for 1 h at 40 °C. After adding the PHSE (20 mg), 1M NaOH solution was added dropwise to the mixture. To form a white precipitate of nanoparticles, the resulting mixture was placed on the heater for 2 to 3 h. Sediment (ZnO-NPs) was collected by centrifugation (8000

rpm, 20 min) and then dried at 80 °C for 2 h.

Ag-NPs synthesis

To synthesize silver nanoparticles, 0.85 g of silver nitrate was added to 500 mL of DW and after adding 20 mg of the PHSE, it was placed on the stirrer (3 h at 37 °C). The NPs were centrifuged and dried at 80 °C for 2 [35, 36].

Identification of Ag and ZnO-NPs

The size and dispersion index (PSI) of NPs were evaluated by the DLS method and then XRD assay was used to evaluate the crystal structure and phase of pure Ag and ZnO-NPs. FTIR spectroscopy was applied to verify the NPs' formation, features, and interactions [37]. The size and morphology of NPs were evaluated by FESEM. For this purpose, a drop of nanoparticles (1mg / 10mL distilled water) was sprayed on a special grade and after drying and coating, it was examined microscopically.

Cell culture

The PC3, A2780, and HepG2 as cancer cells and HFF as non-cancerous normal cells were seeded at the 8×10^4 cells/cm² density in special cell culture media (RPMI or DMEM) at 37 °C. The media was supplemented by FBS, streptomycin, and penicillin in the required proportion.

MTT assay

For this purpose, 5×10^3 cells in each well of 96-well plates were cultured for 24 h and after that, the cells were exposed to serial doses (3.9, 7.8, 15.6, 31.2, and 62.5 $\mu\text{g}/\text{mL}$) of NPs. After 48 h, the culture media of each treated group was refreshed with fresh media supplemented with MTT (0.5 mg/mL). The cells were incubated (3 h at 37 °C) and next, the MTT solution was replaced with 100 μL of DMSO. The OD of the sample was recorded at 570 nm and used for calculating the viability of the cells using the following formula:

$$\text{Cell viability (\%)} = (\text{OD sample}/\text{OD control}) \times 100$$

The test was performed in triplicate.

Anti-oxidant assay

ABTS assay

The anti-oxidant potential of Ag and ZnO nanoparticles was assessed by determining their ability to reduce the ABTS free radicals [38]. Briefly, ABTS solution was made by adding potassium

persulfate and ABTS in a proportion of 2.45 mM: 7 mM in distilled water (1:1). The solution was incubated for 16 h at room temperature (RT) and diluted with DW. The absorbance of the diluted solution was recorded at ~ 0.700 in 734 nm wavelength. Then, the diluted solution of ABTS was mixed with a range of nanoparticles concentrations (0.5, 1, 1.5, 2, and 2.5 mg/mL) with equal volume and incubated for 1h in dark conditions at RT; finally, the absorbance of ABTS was read at 734 nm. The test was performed in triplicate.

DPPH assay

For this, an ethanolic solution of DPPH (1 mg/16 mL) was made and mixed with different concentrations of NPs (0.5, 1, 1.5, 2, and 2.5 mg/mL) in equal volumes. Then, the solution was incubated for 30 min in dark at room temperature and, the absorbance of the sample was read at 517 nm. The anti-oxidant activity of NPs was measured by using the following equation:

$$\text{Antioxidant activity} = \frac{\text{Sample OD} - \text{Control OD}}{\text{Control OD}} \times 100$$

The test was performed in triplicate.

FRAP assay

The anti-oxidant potential of Ag and ZnO nanoparticles was studied by detecting their reductive potential for producing ferrous from ferric ions. According to the Benzie and Strain protocol [39], the solution called FRAP was prepared by mixing tripyridyltriazine (TPTZ), HCL, acetate buffer, and FeCl₃.6H₂O in a proportion of 10 mL: 40 mM: 300 mM: 20 mM at 37 °C. Finally, different doses of nanoparticles (1, 2, 4, 8, 16, and 32 mg/mL) were mixed with the FRAP solution in a ratio of 20:280 µl. The standard curve was prepared regarding the FeSO₄ absorbance of several standard doses at 593 nm [40]. Then, after 30 min incubation in FRAP solution, the absorbance of both ZnO- and Ag-NPs was recorded. The FRAP values were expressed as the produced ferrous ions (mg) for each concentration of nanoparticles (mg). All the measurements were carried out in a triplicate manner.

ROS assay

ROS is naturally produced in cells as a byproduct of oxygen metabolism. Increasing the amount of ROS due to environmental pressures

causes damage to macromolecules and cellular structures and causes oxidative stress. In this study, due to the high sensitivity of A2780 cells to both nanoparticles, this cell line was used to evaluate the amount of intracellular ROS. For this, cells were cultured in 96-well plates and 48 h after treatment with various doses of NPs were prepared according to the protocol of the ROS kit, and finally, the fluorescence intensity was measured (excitation 480-500 nm and emission 510-550 nm) [41]. The test was performed in triplicate.

Anti-angiogenesis activity of Ag and ZnO-NPs

CAM assay

The anti-angiogenesis potential of NPs was analyzed by performing the CAM assay. Briefly, 64 fertilized Ross chicken eggs were divided into 8 groups (N=8). The eggs were stored at 37 °C for 48 h in 55-70% humidity. Then, a 1-cm² window was cut on the shell of the eggs and sealed with sterilized paraffin. Samples were treated with various doses of NPs (125, 250, and 500 µg/mL) on the eighth day as following treatment plan:

- Control group: no treatment
- Lab control: treating with PBS (0.1 M)
- Experimental groups: treating with different doses of both NPs

Finally, the eggs were resealed and incubated for 72 h. The number and length of the CAM blood vessels were measured utilizing stereomicroscopic photos and ImageJ software. Calipers and scales were used to measure the height and weight of the fetuses [42]. The test was performed in triplicate.

Gene expression profile

The anti-angiogenic activity of both NPs was measured on the chorioallantoic membrane tissue of the treated eggs. For this purpose, chorioallantoic membranes were separated from the eggs and pulverized in separate groups with liquid nitrogen. Then, using the bioteck kit, their total RNA was extracted and the amount of RNA in each group was evaluated by the Nanodrop method. Then a certain concentration of RNA was used to synthesize cDNA. The resulting cDNA with cyber green, specific primer, and deionized distilled water to evaluate the expression of VEGF and VEGFR as angiogenesis genes were examined by a qPCR device (Bio-Rad CFX96). The primer list was in Table 1.

Table 1. List of primers used for real-time qPCR

Gene	Forward	Reverse
GAPDH	TGCTGGTGCTGAGTATGTCG	GCATGTCAGATCCACAACGG
VEGF	CTGCTGTCTTGGGTGCATTG	TTCACATTTGTTGTGCTGTAG
VEGFR	TATGTCTATGTTCAAGATTAC	AAGTTTCTTATGCTGATGCTT

Statistical study

For the CAM method, imageJ software was used and then the data obtained from different experiments were analyzed with SPSS software version 21. One-way ANOVA and LSD tests were used to evaluate the significance level of the results. The less than 0.05 p-values were assigned as the significant levels.

RESULTS

Identification of Ag-NPs

The Z-average and PDI values of Ag-NPs were estimated at 82.42 nm and 0.25, respectively, which make the Z-average a reliable size index regarding Stetefeld’s theory (Fig. 1A). The theory demonstrates that less than 0.7 PDI values refer to the mono-distribution condition [43]. Also, the XRD algorithms show the crystal features Ag-NPs (Fig. 1B). The individual pecks of Ag-NP crystals are observable at 32 and 54 2θ-degrees. FE-SEM micrographs of Ag-NPs indicate its pseudo spherical morphology, support the DLS data and approve

their estimated D mean number values (Fig. 1C). FTIR spectrum of Ag-NPs expressed visible bands at 3314.84 (O–H and N–H stretching), 2923.14 and 2847.67 (C–H stretching), 1691.26 and 1596.60 (N–H stretching), 1454.26 and 1357.90 (C–H stretching), 1245.86 (C–C(=O)–O stretching), 1156.0 (asymmetric stretching of the C–O–C), 1066.18 (C–O stretching), and The peak at 602.96 cm⁻¹ is attributed to the bonding of oxygen from the O–H groups [44]. The FTIR data (Fig. 1D) indicates that the biological molecules could be involved in the synthesis and stabilization of Ag-NPs.

Characterization of ZnO-NPs

The DLS data exhibited the formation of ZnO-NPs with a size of 163.05 nm and PDI of 0.25. Since colloidal particles with a dispersion index of 0-0.7 are introduced as particles with uniform dispersion, so ZnO-NPs can be considered monodisperse particles (Fig. 1A). FESEM results confirm the presence of spherical particles with a rough appearance and size of about 100 nm, which is consistent with the data from DLS (Fig. 2B). The

Characterization

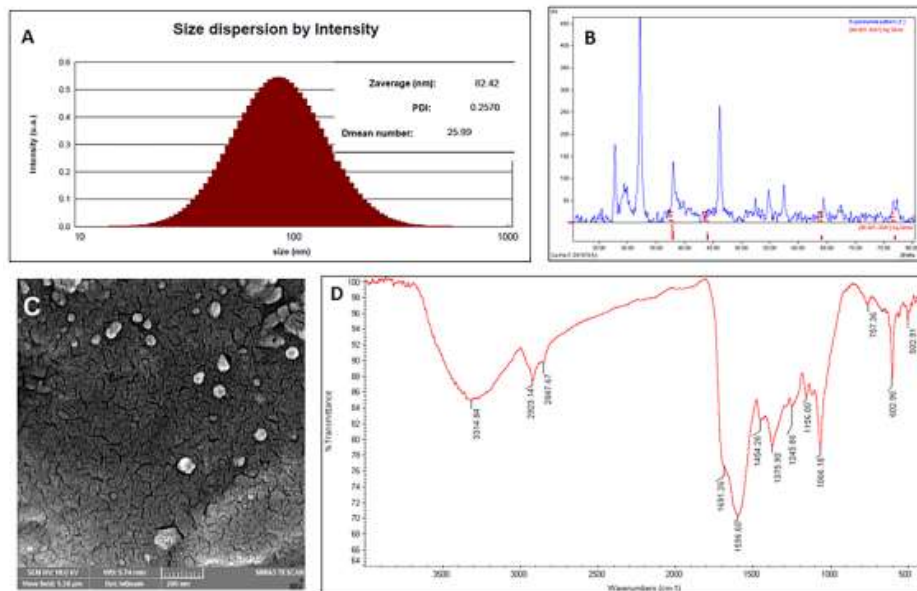


Fig. 1. The Ag-NPs characterization results. (A) The Z-average and PDI indices were defined at 82.42 nm and 0.25, respectively. (B) The XRD pattern of Ag-NPs. (C) The FESEM image of Ag-NPs. (D) The FTIR diagram indicates the chemical characteristics of Ag-NPs

Characterization

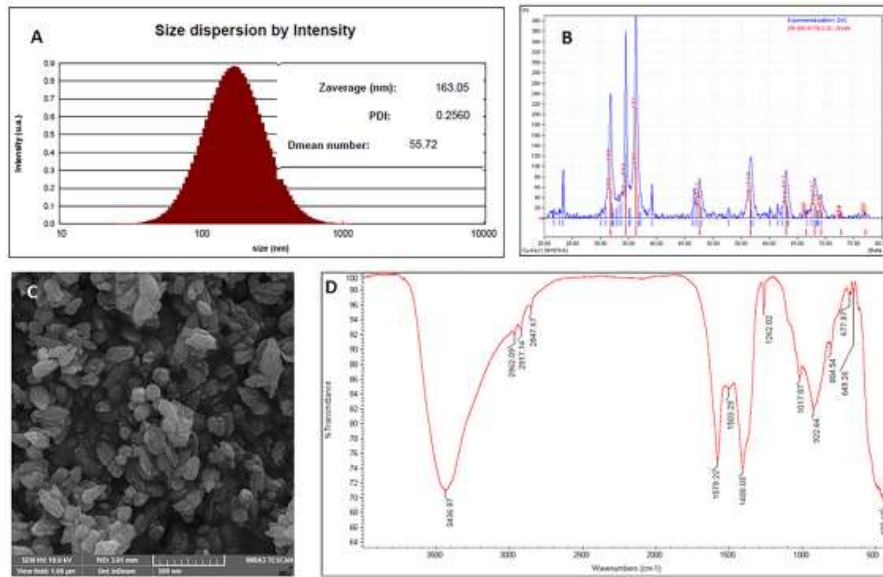


Fig. 2. The ZnO-NPs characterization data. (A) The Z-average and PDI indices were defined at 163.05 nm and 0.25, respectively. (B) The XRD pattern of ZnO-NPs. (C) The FESEM image of ZnO-NPs. (D) The FTIR diagram indicates the chemical properties of the ZnO-NPs crystal structure

XRD algorithm of ZnO-NPs (the specific picks for 2θ values in the range of 30 to 40 degrees) (Fig. 2C) verified their synthesis. The chemical features of ZnO-NPs were defined by two specific lowest and highest wavenumbers at 435.18 cm^{-1} and 3436.97 cm^{-1} , respectively (Fig. 2D). The sharp peak at 435.18 cm^{-1} corresponding to the Zn–O stretching bond. The absorption peaks at the range of $1700\text{ to }600\text{ cm}^{-1}$ attributed to C=O, C–O, and C–H vibrations respectively. Other peaks are due to the hydroxyl stretching vibrations and bending modes of the adsorbed water [45].

The cytotoxicity of Ag-NPs

The effect of concentration-dependent toxicity of silver nanoparticles against cancer cell lines compared to normal is shown in Fig. 3A shown in the diagram (Fig. 3A), prostate cancer cells show the highest resistance to treatment, while ovarian and liver cancer cells are the highest sensitive to treatment. Ag-NPs reduced only HepG2 and A2780 cancer cells in lower than its IC_{50} doses for normal HFF cells (Fig. 3B). Therefore, the safe toxic doses (STD) of Ag-NPs are defined at lower the $19.23\text{ }\mu\text{g/mL}$.

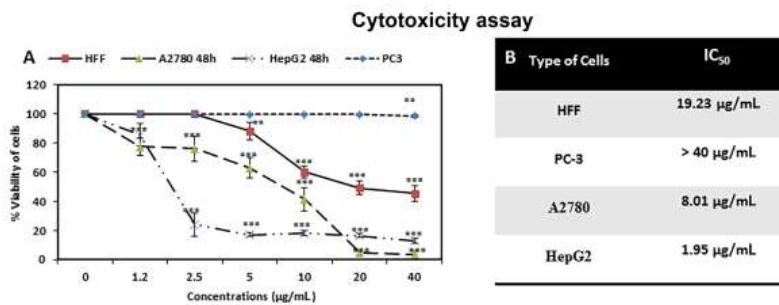


Fig. 3. Cytotoxic effects of Ag-NPs. (A) the diagrams indicate the cancer cells' viability following treatment with different Ag-NPs concentrations after 48 h. (N= 3), $**P<0.01$ and $***P<0.001$. (B) Medium concentrations (IC_{50}) of Ag-NPs against different cell lines. The test was performed in triplicate

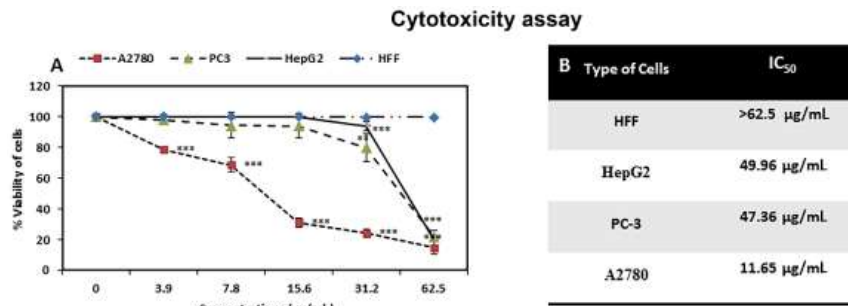


Fig. 4. The cytotoxic activity of ZnO-NPs. (A) the diagrams indicate the cancer cells' viability following various ZnO-NPs concentrations (N= 3), *** P<0.001. (B) Medium concentrations (IC₅₀) of ZnO-NPs against different cell lines. The test was performed in triplicate

The cytotoxicity of ZnO-NPs

The results MTT assay showed that ZnO-NPs can inhibit all three cancer lines in a dose-dependent way (Fig. 4A). No inhibitory effect against normal cells was reported at the concentrations studied. Examination and comparison of IC₅₀ showed that nanoparticles inhibited A2780, HepG2, and PC3 cells with moderate concentrations of 11.65, 47.36, and 49.96 µg/mL, respectively (Fig. 4B). Thus, the A2780 cell showed the highest sensitivity to ZnO-NPs treatment compared to other cells.

Anti-oxidant capacity of Ag-NPs

Fig. 5A demonstrates the potential of Ag-NPs to reduce iron ions compared to FeSO₄ as a standard anti-oxidant. According to Fig, the FRAP value increases with increasing concentration of Ag-NPs, and its highest value (0.14) is observed at a concentration of 4 mg / mL Ag-NPs.

Therefore, it can be said that nanoparticles at a concentration of 4 mg / mL 0.1 FeSO₄ can reduce iron ions. The concentration-dependent inhibitory effects of Ag-NPs against ABTS and DPPH free radicals are shown in Fig 5B. As can be seen, nanoparticles can inhibit 50% of ABTS free radicals at a concentration of about 200 µg/mL, while the median concentration for inhibiting DPPH free radicals is about 707.3 µg/mL. Therefore, the results show higher inhibitory effects of nanoparticles on ABTS free radicals compared to DPPH. Evaluation of changes in intracellular ROS in Ag-NPs treatment was measured by absorption method (5C). The results showed a significant increase in the amount of intracellular ROS in the treated cells with a concentration of 2 mg / mL. As the concentration of the treatment increases, the amount of intracellular ROS increases dramatically, this confirms the role of Ag-NPs in inducing cell

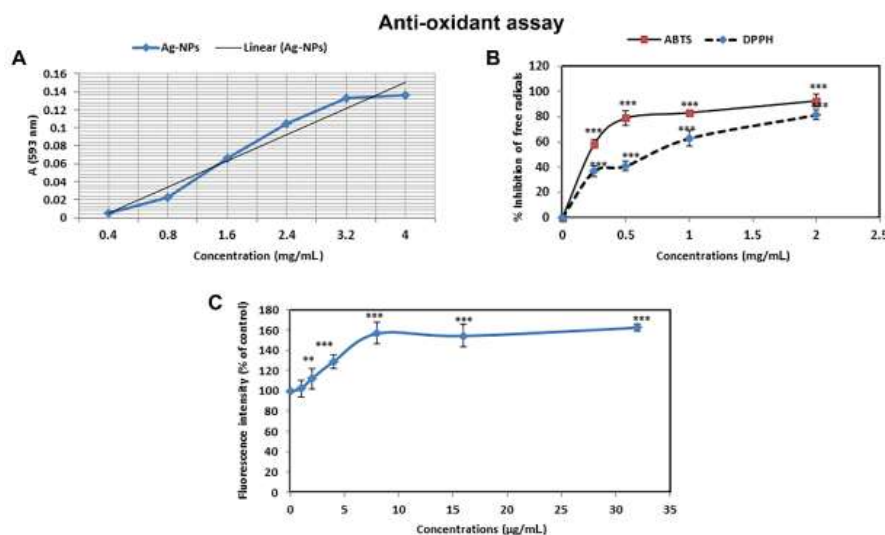


Fig. 5. The Ag-NPs antioxidant activity. (A) The FRAP assay data. (B) Scavenging of ABTS and DPPH free radicals with nanoparticle exposure (C) Improved intracellular ROS production in Ag-NPs -treated cells. (N= 3) and ***P<0.001. The test was performed in triplicate

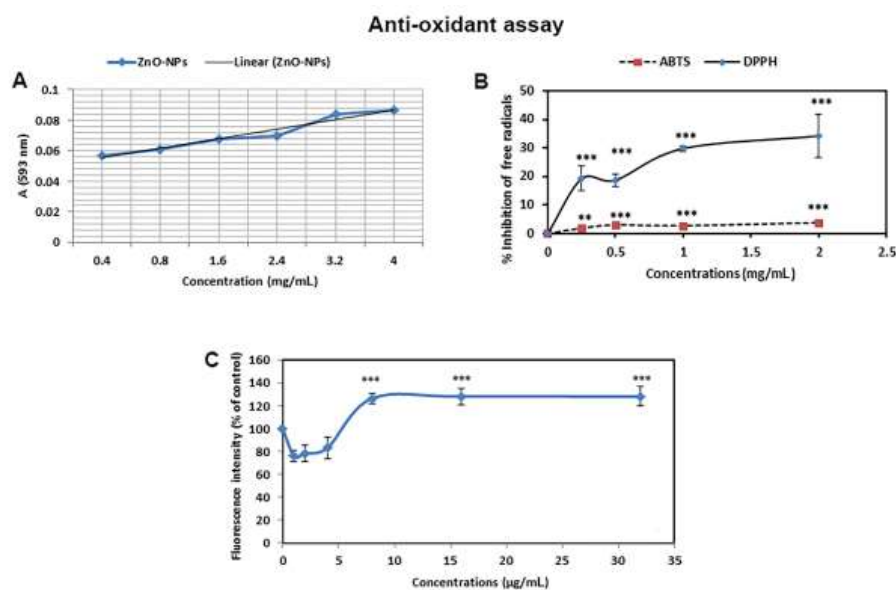


Fig. 6. The ZnO-NPs antioxidant properties. (A) Ferric Reducing Antioxidant Power (FRAP) of the ZnO-NPs. (B) Scavenging of ABTS and DPPH free radicals with ZnO-NPs exposure (C) Enhanced intracellular ROS production in ZnO-NPs-treated cells. (N= 3) and *** $P < 0.001$. The test was performed in triplicate

death by increasing intracellular ROS and causing oxidative stress damage [41].

Anti-oxidant capacity of ZnO-NPs

The reducing power of iron ions in the presence of ZnO-NPs compared to FeSO₄ was evaluated by the FRAP method. The results showed that nanoparticles at the highest concentration can inhibit iron ions with a FRAP value of about 0.1 (Fig. 6A). The inhibitory effect of ZnO-NPs on ABTS and DPPH free radicals was evaluated to evaluate the anti-oxidant power of ZnO-NPs. As shown (Fig. 6B), increasing the concentration of ZnO-NPs increases the inhibition rate, and the highest percentage of inhibition for ABTS free radicals is reported at a concentration of 2 mg / mL ZnO-NPs of about 4%. While at similar concentrations, about 34.25% of DPPH free radicals were inhibited. These results confirm the moderate inhibitory potency of ZnO-NPs against DPPH free radicals. One of the most important features of anti-cancer compounds is their ability to induce intracellular ROS, followed by cell damage and induction of cell death. In this study, intracellular ROS changes were evaluated in cells treated with different concentrations of ZnO-NPs. The results showed a significant increase in ROS in treated cells with a concentration of 8, 16, and 32 µg/mL (Fig. 6C).

Anti-angiogenesis potential of Ag-NPs

Fig. 7A shows the images of the treated area in the experimental groups compared to the control. As can be seen, the images clearly show the reduction of blood vessels in the treated groups with 250 and 500 µg/mL of Ag-NPs. Examination of the mean number of blood vessels in the control laboratory control and samples treated with a concentration of 125 µg/mL Ag-NPs did not show a statistically significant difference ($P > 0.05$). However, by increasing the concentration to 250 ($*P < 0.05$) and 500 µg/mL ($***P < 0.001$), a significant decrease in the number of blood vessels is observed. Significant reduction in blood vessel length was also observed only in treated samples with concentrations of 250 ($**P < 0.01$) and 500 µg/mL ($***P < 0.001$). Examination of fetal height and weight in experimental groups compared to control shows that only in samples treated with a concentration of 500 µg/mL there is a significant reduction ($*P < 0.05$) (Fig. 7B). Examination of alterations in the expression of angiogenesis-related genes in Ag-NPs-treated samples showed that the VEGFR gene was significantly reduced in all concentrations studied, while the expression of the VEGF gene at both concentrations of 125 and 250 µg/mL is approximately constant and similar to the control group, while in the samples treated

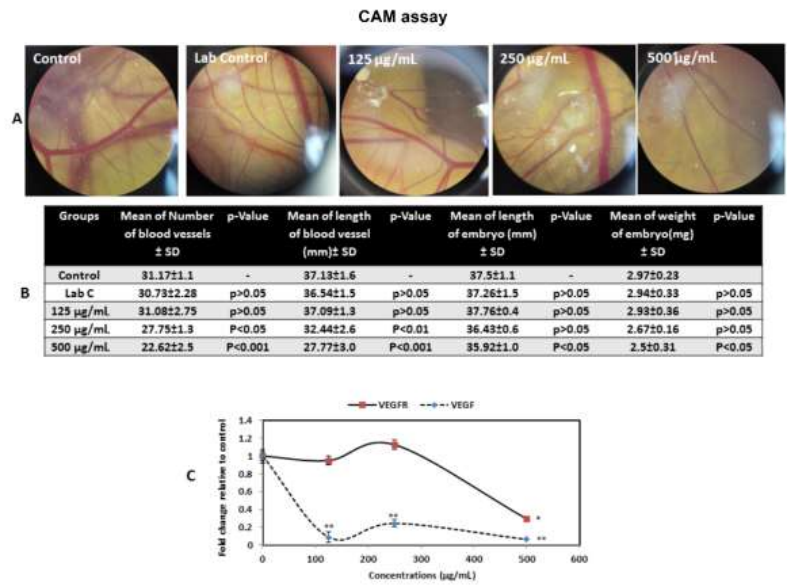


Fig. 7. CAM assay (A) The stereomicroscopic micrograph of CAM following the treatment with different doses of Ag-NPs, (B) Decrease in mean number and length of blood vessels and also changes in fetal growth factors (height and weight) following the treatment with different doses of Ag-NPs (N= 8); (* P<0.05, ** P<0.01, *** P<0.001). (C) Change in VEGF and VEGF-R gene expression in Ag-NPs-treated samples compared to control. Data are significant at the level of * P<0.05 and *** P<0.001 (N=3). The test was performed in triplicate

with a concentration of 500 µg/mL, its expression was significantly reduced (Fig. 7C).

Anti-angiogenesis properties of ZnO-NPs

Microscopic changes of vessels in nanoparticle-treated samples compared to the control are

shown in Fig 8A. As can be seen, the amount of blood vessels in the experimental groups is almost similar to the control sample. To further evaluate the effect of nanoparticles on angiogenesis, the mean length and number of blood vessels were evaluated with Imag J software and the results

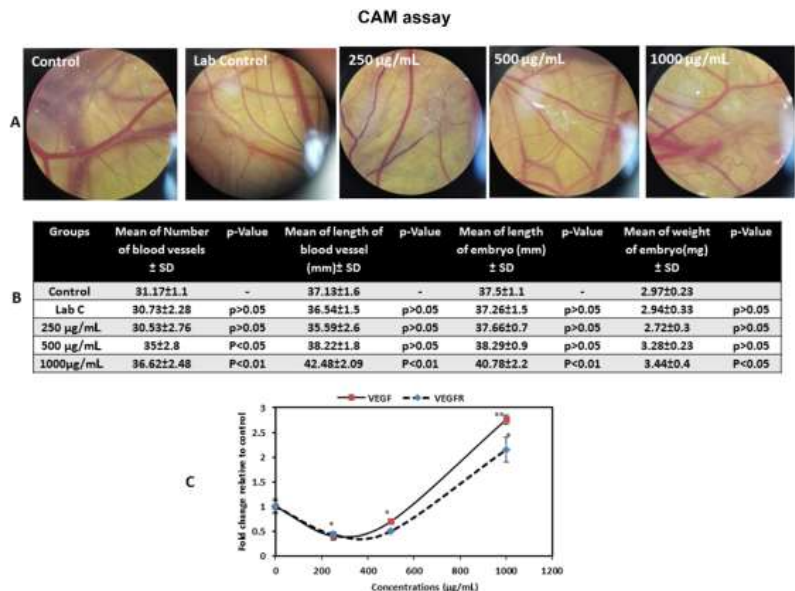


Fig. 8. CAM assay (A) The stereomicroscopic micrograph of CAM following the treatment with different doses of ZnO-NPs, (B) Change in mean number and length of blood vessels and embryonic growth factors in ZnO-NPs treatment (N= 8); (* P<0.05, ** P<0.01, *** P<0.001). (C) Change in VEGF and VEGF-R gene expression in ZnO-NPs-treated samples compared to control. * P<0.05 and ** P<0.01 (N=3). The test was performed in triplicate

exhibited an increase in the average number of blood vessels in the two treated groups 500 (* $P < 0.05$) and 1000 $\mu\text{g}/\text{mL}$ (** $P < 0.01$). While the average length of blood vessels showed an increase only in the 1000 $\mu\text{g}/\text{mL}$ (** $P < 0.01$) treated group. An increase in the mean length (** $P < 0.01$) and weight (* $P < 0.05$) of the embryos during the increase in vascular factors was observed only in samples treated with 1000 $\mu\text{g}/\text{mL}$ (Fig. 8B). In order to evaluate the NPs effect on angiogenesis at the molecular level, the expression of VEGF and VEGFR genes was evaluated by qPCR method. As can be seen, at two concentrations of 250 and 500 $\mu\text{g}/\text{mL}$, a significant decrease in the expression of genes associated with angiogenesis is observed, but with increasing the concentration of treatment to 1000 $\mu\text{g}/\text{mL}$, the expression of genes increases significantly (Fig. 8C). Considering the alteration in the expression of angiogenesis-related genes and the results of the CAM test, it can be said that the effect of ZnO-NPs on angiogenesis was dose-dependent. In such a way that at low concentrations at the molecular level, it inhibits angiogenesis, and by increasing the concentration, its effect on angiogenesis is reversed. Therefore, to use these nanoparticles in studies related to cancer treatment, it is important to pay attention to the concentration used.

DISCUSSION

The genotype complexity and poor prognosis of cancer are considered the main barriers to its treatment. The use of nanotechnology as a practical field to develop effective methods in the diagnosis and treatment of cancer has been considered by many researchers today [46]. Metal and metal oxide NPs such as Ag and ZnO-NPs play a prominent role in biomedical applications [47, 48]. Due to the growing burden of cancer worldwide, different types of metal NPs have been fabricated through the green approach. For example, ZnO-NPs have been fabricated by various types of bio-platforms such as *Laurus nobilis* [49], *Deverra tortuosa* [50], *Garcinia mangostana* fruit [51], and *Cucumis melo inodorus* rough shell extracts [52]. Also, several types of plant extracts have been utilized for synthesizing Ag-NPs including *Amphipterygium adstringens* [53], *Centella Asiatica* [54], and *Ficus benghalensis* prop root extracts [55]. In the current study, Pecan smoke extract (PHSE) was used as a biological platform for the green synthesis of ZnO and Ag-NPs, and

then the biological effects of NPs were investigated and compared. Smoke from burning pecan seeds has been shown to have anti-cancer properties. However, very few studies have examined this phenomenon. *P. harmala* smoke extract was evaluated in comparison with normal cells and it was shown that it inhibited breast cancer cells more effectively than HFF cells [56]. The use of biological systems such as plant extracts and metabolites as reducing and stabilizing agents for the fabrication of NPs is called the green synthesis method [57], which has been successfully used in cancer treatment approaches and is an effective step in eliminating the disadvantages of physical and chemical methods [58].

In this study, smoke from burning *Peganum Harmala* seeds was used to green synthesize silver (25.99 nm and PDI: 0.25) and zinc oxide (55.72 nm and PDI: 0.25) nanoparticles. In a study in 2015, Ag-NPs with a size of 5 to 25 nm from the aqueous extract of *Caulerparacemosa* were prepared by the green method [59]. In another study, Ag-NPs were green synthesized using the sumac aqueous extract with an average size of 35 nm [60] which is comparable to the Ag-NPs synthesized in the present study. Similar to the present study, in a study conducted in 2021, globular nanoparticles with 55 nm were fabricated by the green method. In this study, *Arthrospira platensis* was used as a reducing agent for the formation of NPs [61].

FTIR spectroscopy provides valuable information due to the excitation of specific fundamental vibrational transitions characteristic of functional groups in molecules. NPs of diverse natures have been characterized using spectroscopic techniques in the infrared range. NPs with inherent infrared absorptions or functional groups present at their surface may thus be directly characterized via infrared spectroscopy. Furthermore, different ligands attached to nanoparticles may readily be identified according to their vibrational signatures in a rapid, precise, and non-destructive way. Next to the direct characterization of such materials, some nanostructures modify the local optical field, yielding enhanced IR signals and facilitating advanced IR imaging procedures for NPs [62].

In this study, the toxicity of Ag-NPs and ZnO-NPs against three cancer cell lines was compared with HFF cells. The most sensitive and resistant cell lines to treatment with Ag-NPs were HepG2 and PC3 with IC_{50} about 1.95 and above 40 $\mu\text{g}/\text{mL}$, respectively, while in the treatment with ZnO-NPs

the highest and lowest resistance to treatment in HFF and A2780 cells with IC_{50} higher than 62 $\mu\text{g}/\text{mL}$ and 11.65 $\mu\text{g}/\text{mL}$ (respectively) was observed. Since ZnO-NPs did not show any toxic effect on normal cells at the studied concentrations, it can be said that ZnO-NPs are safer compared to Ag-NPs. Many studies similar to our study have shown the toxicity of various NPs including Ag-NPs and ZnO-NPs on cancer cells. A study in 2018 showed higher cytotoxic effects of Ag-NPs synthesized from *Artemisia tournefortiana* extract against HT-29 ($IC_{50}=40.71 \text{ mg}/\text{mL}$) compared to the HEK293 ($IC_{50}=61.38 \text{ mg}/\text{mL}$) as normal cells [63]. In another study was reported the strongly cytotoxic effects of Ag-NPs synthesized by aqueous extract of *Rubia tinctorum* against HepG-2 cells (IC_{50} : 6 $\mu\text{g}/\text{mL}$) compared to the HFF (IC_{50} : 100 $\mu\text{g}/\text{mL}$) as normal cells [64]. A study conducted in 2021 on the fabricated ZnO-NPs by *Swertia chirayita* leaf extract revealed the toxic effects against HCT-116 and Caco-2. The nanoparticles showed a strong cytotoxic potency against HCT-116 and Caco-2 cell lines, but less so against the normal HEK-293 cell line [65]. Also, in a study in 2019, Mahdizadeh et al. reported the toxicity of ZnO-NPs from *Cucumis melo* on MCF7 (40 $\mu\text{g}/\text{mL}$) and Tubo (20 $\mu\text{g}/\text{mL}$) cells after 24 h [52].

ROS increasing, although under natural conditions causes diseases related to oxidative stress such as cancer, in the treatment of cancer is used as one of the applied strategies in chemotherapy [25]. Studies show that increasing the amount of ROS can lead to the release of cytochrome C and activation of the apoptotic pathway by changing the permeability of the mitochondrial membrane [66]. Our findings show the anti-oxidant effect of ZnO and Ag-NPs in vitro and its pro-oxidant effects inside the cancer cell. Our results exhibited a significant anti-oxidant capability for Ag-NPs for ABTS (IC_{50} :150.07 $\mu\text{g}/\text{mL}$) and DPPH (IC_{50} : 707.33 $\mu\text{g}/\text{mL}$) free radicals (Fig 5). In other words, ZnO-NPs appeared as a weak radical scavenger compared with Ag-NPs and glutathione anti-oxidant potential.

In 2019, Ahmadi et al reported the inhibitory effect of ZnO-NPs against ABTS and DPPH free radicals with IC_{50} about 31.2 and 60 $\mu\text{g}/\text{mL}$ [67], which shows a higher anti-oxidant power compared to our study. Similar to the present study, in a 2015 study, the inhibitory effects of Ag-NPs from *Cassia roxburghii* on ABTS free radicals (IC_{50} : 140 $\mu\text{g}/\text{mL}$) and their reducing power on

iron ions (FRAP of 2.64 (Mg^{-1})) were investigated and confirmed [68]. Also, in a study in 2017, 23-95% of ABTS free radical scavenging capacity and 8.8 Mg^{-1} FRAP activities of Ag-NPs were reported [69]. The results of many studies show that NPs increase ROS production in various cancer cells [30]. Similar to the present study, in a 2020 study, the anti-proliferative and pro-oxidant effects of Ag-NPs from *Beta vulgaris L* were demonstrated in human hepatic cancer cells (HUH7) by ROS induction[70]. Lee et al. reported the potential to stimulate ROS production in human keratinocytes treated with ZnO-NP. They showed that the mechanism of nanoparticle toxicity is related to ROS production, oxidative stress, and apoptosis [71]. In another study in 2017, Bai et al. exhibited increasing intracellular ROS in SKOV3 treated with ZnO-NPs [72].

Angiogenesis is one of the most important features of tumor cells that help their survival and reducing angiogenesis plays the main role in preventing the growth of cancer cells and inflammation [30]. The results of this survey confirmed the reduction of angiogenesis in the treatment with different concentrations of Ag-NPs in CAM and qPCR assay. Investigation of the effect of ZnO-NPs on angiogenesis showed that they suppress angiogenesis by down-regulating VEGF and VEGFR gene expression at 0 to 500 $\mu\text{g}/\text{mL}$ concentrations and act as a pro-angiogenic compound at >500 $\mu\text{g}/\text{mL}$ doses. In many studies consistent with the present investigation, the anti-angiogenesis effects of nanoparticles have been investigated and confirmed [73, 74]. A reduction in angiogenesis by the CAM method was reported in a 2015 study by examining the mean number and length of blood vessels in samples treated with Ag-NPs [22]. It has also been reported that Ag-NPs inhibit the expression of VEGF in mouse Matrigel plugs and retinal endothelial cells [73, 75]. Various investigations have shown the anti and pro-angiogenesis potential of ZnO-NPs. In a study in 2019, the anti-angiogenesis effects of ZnO-NPs from *Hyssops officinalis L* were reported using the CAM assay [21]. Ahtzaz et al reported the pro-angiogenic effects of ZnO-NPs in 2017 using the CAM method [31]. In a study by Oikawa et al., The inhibitory effect of ZnO-NPs on the formation of blood vessels by reducing the expression of VEGF and VEGFR was reported [76] which is comparable to our results.

CONCLUSION

The results of this study clearly showed an

increase in the effectiveness of PSE loaded in synthesizing Ag-NPs and ZnO-NPs as anticancer agents in vitro. NPs had uniform dispersion and showed the effects of selective toxicity on cancer cells compared to normal cells. According to the results, Ag-NPs exhibited stronger anti-oxidant capacity than ZnO-NPs. In addition, Ag-NPs showed significant anti-angiogenesis effects by reducing VEGF and VEGFR gene expressions. Considering the survival of cancer cells and suppression of angiogenesis, higher anti-cancer activity of Ag-NPs was detected compared to ZnO-NPs.

ACKNOWLEDGMENTS

The authors very much appreciate the support provided by the Islamic Azad University, Tehran, Iran, in the conducting of the present research.

FUNDING

The present work was funded by Islamic Azad University, Tehran, Iran. The university's support of this research is very much appreciated by the authors.

DATA AVAILABILITY STATEMENT

The data that support the findings of this study are available upon reasonable request from the authors.

CONFLICTS OF INTEREST

The authors report no conflict of interest.

REFERENCES

1. Martínez-Vieyra C, Olguin M, Gutiérrez-Segura E, López-Tellez G. Comparison of Ag, Cu and Zn nanoparticles obtained using Aloe vera extract and gamma ionizing radiation. *J Appl Res Technol*. 2020;18(5):289-314.
2. Raghunandan D, Ravishankar B, Sharanbasava G, Mahesh DB, Harsoor V, Yalagatti MS, et al. Anti-cancer studies of noble metal nanoparticles synthesized using different plant extracts. *Cancer Nanotechnol*. 2011;2(1):57-65.
3. Banerjee D, Harfouche R, Sengupta S. Nanotechnology-mediated targeting of tumor angiogenesis. *Vascular Cell*. 2011;3(1):1-13.
4. Singh BN, Rawat AKS, Khan W, Naqvi AH, Singh BR. Biosynthesis of stable antioxidant ZnO nanoparticles by *Pseudomonas aeruginosa* rhamnolipids. *PLoS One*. 2014;9(9):e106937.
5. Jesionowski T. Zinc oxide—from synthesis to application: a review. *Materials*. 2014;7:2833-2881.
6. Rasmussen JW, Martinez E, Louka P, Wingett DG. Zinc oxide nanoparticles for selective destruction of tumor cells and potential for drug delivery applications. *Expert Opin Drug Deliv*. 2010;7(9):1063-1077.
7. Nasrollahzadeh MS, Ghodsi R, Hadizadeh F, Maleki M, Mashreghi M, Poy D. Zinc oxide nanoparticles as a potential agent for antiviral drug delivery development: A systematic literature review. *Curr Nanosci*. 2022;18(2):147-1453.
8. Zhang Z-Y, Xiong H-M. Photoluminescent ZnO nanoparticles and their biological applications. *Materials*. 2015;8(6):3101-3127.
9. Xiong HM. ZnO nanoparticles applied to bioimaging and drug delivery. *Adv Mater*. 2013;25(37):5329-5335.
10. Burdușel A-C, Gherasim O, Grumezescu AM, Mogoantă L, Fica A, Andronescu E. Biomedical applications of silver nanoparticles: an up-to-date overview. *Nanomaterials*. 2018;8(9):681.
11. Wei L, Lu J, Xu H, Patel A, Chen Z-S, Chen G. Silver nanoparticles: synthesis, properties, and therapeutic applications. *Drug Discov Today*. 2015;20(5):595-601.
12. Es-haghi A, Mashreghi M, Rezaade Bazaz M, Homayouni-Tabrizi M, Darroudi M. Fabrication of biopolymer based nanocomposite wound dressing: evaluation of wound healing properties and wound microbial load. *IET Nanobiotechnol*. 2017;11(5):517-522.
13. Mousavi-Kouhi SM, Beyk-Khormizi A, Amiri MS, Mashreghi M, Yazdi MET. Silver-zinc oxide nanocomposite: From synthesis to antimicrobial and anticancer properties. *Ceram Int*. 2021;47(15):21490-21497.
14. Thunugunta T, Reddy AC, DC LR. Green synthesis of nanoparticles: current prospectus. *Nanotechnol Rev*. 2015;4(4):303-323.
15. Ananthalakshmi R, Rajarathinam S, Sadiq AM. Antioxidant activity of ZnO Nanoparticles synthesized using *Luffa acutangula* peel extract. *Res J Pharm Technol*. 2019;12(4):1569-1572.
16. Tanase C, Berta L, Coman NA, Roșca I, Man A, Toma F, et al. Antibacterial and antioxidant potential of silver nanoparticles biosynthesized using the spruce bark extract. *Nanomaterials*. 2019;9(11):1541.
17. Gomes HI, Martins CS, Prior JA. Silver nanoparticles as carriers of anticancer drugs for efficient target treatment of cancer cells. *Nanomaterials*. 2021;11(4):964.
18. Zhang T, Du E, Liu Y, Cheng J, Zhang Z, Xu Y, et al. Anticancer effects of zinc oxide nanoparticles through altering the methylation status of histone on bladder cancer cells. *Int J Nanomedicine*. 2020;15:1457.
19. Siddiqi KS, ur Rahman A, Husen A. Properties of zinc oxide nanoparticles and their activity against microbes. *Nanoscale Res Lett*. 2018;13(1):1-13.
20. Talapko J, Matijević T, Juzbašić M, Antolović-Požgain A, Škrlec I. Antibacterial activity of silver and its application in dentistry, cardiology and dermatology. *Microorganisms*. 2020;8(9):1400.
21. Mohammad GRKS, Tabrizi MH, Ardalan T, Yadamani S, Safavi E. Green synthesis of zinc oxide nanoparticles and evaluation of anti-angiogenesis, anti-inflammatory and cytotoxicity properties. *J Biosci*. 2019;44(2):1-9.
22. Khandia R, Munjal A, Bangrey R, Mehra R, Dhama K, Sharma N. Evaluation of silver nanoparticle mediated reduction of neovascularisation (angiogenesis) in chicken model. *Adv Anim Vet Sci*. 2015;3(7):372-376.
23. Wang EC, Wang AZ. Nanoparticles and their applications in cell and molecular biology. *Integ Biol*. 2014;6(1):9-26.
24. Pizzino G, Irrera N, Cucinotta M, Pallio G, Mannino F, Arcoraci V, et al. Oxidative stress: harms and benefits for human health. *Oxid Med Cell Longev*. 2017;2017:8416763.
25. Soltani M, Etminan A, Rahmati A, Behjati Moghadam M, Ghaderi Segonbad G, Homayouni Tabrizi M. Incorporation of *Boswellia sacra* essential oil into chitosan/TPP nanoparticles towards improved therapeutic efficiency. *Mater Technol*. 2021:1-13.
26. Saud Alarifi DA, Alkahtani S, Verma A, Ahamed M, Ahmed M, Alhadlaq HA. Induction of oxidative stress, DNA damage,

- and apoptosis in a malignant human skin melanoma cell line after exposure to zinc oxide nanoparticles. *Int J Nanomedicine*. 2013;8:983.
27. Balkrishna A, Kumar A, Arya V, Rohela A, Verma R, Nepovimova E, et al. Phytoantioxidant Functionalized Nanoparticles: A Green Approach to Combat Nanoparticle-Induced Oxidative Stress. *Oxid Med Cell Longev*. 2021;2021:3155962..
 28. Wang ZL. Zinc oxide nanostructures: growth, properties and applications. *J Phys Condens Matter*. 2004;16(25):R829.
 29. Meulenkamp EA. Synthesis and growth of ZnO nanoparticles. *J Phys Chem B*. 1998;102(29):5566-5572.
 30. Ahmed NH, Said UZ, Meky NH, Mohamed MA. Role of chitosan nanoparticles as anti-angiogenic in mice bearing Ehrlich carcinoma. *Oncol Res Rev*. 2018;1:1-6.
 31. Ahtzaz S, Nasir M, Shahzadi L, Amir W, Anjum A, Arshad R, et al. A study on the effect of zinc oxide and zinc peroxide nanoparticles to enhance angiogenesis-pro-angiogenic grafts for tissue regeneration applications. *Mater Des*. 2017;132:409-418.
 32. Branch S. Etymological review on chemical and pharmaceutical substances of the oriental origin. *Int J Anim Veter Adv*. 2012;4:40-44.
 33. Shabestarian H, Homayouni Tabrizi M, Movahedi M, Neamati A, Sharifnia F. Putative mechanism for cancer suppression by PLGA nanoparticles loaded with Peganum harmala smoke extract. *J Microencapsul*. 2021;38(5):324-337.
 34. Shahverdi A, Ostad S, Khodae S, Bitarafan L, Monsef-Esfahani H, Jamalifar H, et al. Antimicrobial and cytotoxicity potential of Peganum harmala smoke. *Pharmacogn Mag*. 2008;4(15):236.
 35. Ahmed S, Ahmad M, Swami BL, Ikram S. Green synthesis of silver nanoparticles using *Azadirachta indica* aqueous leaf extract. *J Radiat Res Appl Sci*. 2016;9(1):1-7.
 36. Santhoshkumar J, Kumar SV, Rajeshkumar S. Synthesis of zinc oxide nanoparticles using plant leaf extract against urinary tract infection pathogen. *Resource-Efficient Technologies*. 2017;3(4):459-465.
 37. Mishra V, Sharma R. Green synthesis of zinc oxide nanoparticles using fresh peels extract of *Punica granatum* and its antimicrobial activities. *Int J Pharma Res Health Sci*. 2015;3(3):694-699.
 38. Li P, Huo L, Su W, Lu R, Deng C, Liu L, et al. Free radical-scavenging capacity, antioxidant activity and phenolic content of *Pouzolzia zeylanica*. *Glas Hem Drus Beogr*. 2011;76(5):709-717.
 39. Benzie IF, Strain JJ. The ferric reducing ability of plasma (FRAP) as a measure of "antioxidant power": the FRAP assay. *Anal Biochem*. 1996;239(1):70-76.
 40. Rajurkar NS, Hande S. Estimation of phytochemical content and antioxidant activity of some selected traditional Indian medicinal plants. *Indian J Pharm Sci*. 2011;73(2):146.
 41. Thyagarajan A, Sahu RP. Potential contributions of antioxidants to cancer therapy: immunomodulation and radiosensitization. *Integr. Cancer Ther*. 2018;17(2):210-216.
 42. Sanaeimehr Z, Javadi I, Namvar F. Antiangiogenic and antiapoptotic effects of green-synthesized zinc oxide nanoparticles using *Sargassum muticum* algae extraction. *Cancer Nanotechnol*. 2018;9(1):3.
 43. Stetefeld J, McKenna SA, Patel TR. Dynamic light scattering: a practical guide and applications in biomedical sciences. *Biophys Rev*. 2016;8(4):409-427.
 44. Wan Mat Khalir WKA, Shameli K, Jazayeri SD, Othman NA, Che Jusoh NW, Hassan NM. Biosynthesized silver nanoparticles by aqueous stem extract of *Entada spiralis* and screening of their biomedical activity. *Front Chem*. 2020;8:620.
 45. Babu KS, Reddy AR, Sujatha C, Reddy KV, Mallika A. Synthesis and optical characterization of porous ZnO. *J Adv. Ceram*. 2013;2(3):260-265.
 46. Jabeen S, Qureshi R, Munazir M, Maqsood M, Munir M, Shah SH, et al. Application of green synthesized silver nanoparticles in cancer treatment-a critical review. *Mater. Res. Express*. 2021.
 47. Murthy S, Effiong P, Fei CC. Metal oxide nanoparticles in biomedical applications. *Metal Oxide Powder Technologies*: Elsevier; 2020. p. 233-251.
 48. Aalami AH, Mesgari M, Sahebkar A. Synthesis and characterization of green zinc oxide nanoparticles with antiproliferative effects through apoptosis induction and microRNA modulation in breast cancer cells. *Bioinorg Chem Appl*. 2020;2020 :8817110.
 49. Fakhari S, Jamzad M, Kabiri Fard H. Green synthesis of zinc oxide nanoparticles: A comparison. *Green Chem Lett Rev*. 2019;12(1):19-24.
 50. Selim YA, Azb MA, Ragab I, Abd El-Azim MH. Green synthesis of zinc oxide nanoparticles using aqueous extract of *deverra tortuosa* and their cytotoxic activities. *Sci Rep*. 2020;10(1):1-9.
 51. Aminuzzaman M, Ying LP, Goh W-S, Watanabe A. Green synthesis of zinc oxide nanoparticles using aqueous extract of *Garcinia mangostana* fruit pericarp and their photocatalytic activity. *Bull Mater Sci*. 2018;41(2):50.
 52. Mahdizadeh R, Homayouni-Tabrizi M, Neamati A, Seyedi SMR, Tavakkol Afshari HS. Green synthesized-zinc oxide nanoparticles, the strong apoptosis inducer as an exclusive antitumor agent in murine breast tumor model and human breast cancer cell lines (MCF7). *J Cell Biochem*. 2019;120(10):17984-1793.
 53. Rodríguez-Luis OE, Hernandez-Delgadillo R, Sánchez-Nájera RI, Martínez-Castañón GA, Niño-Martínez N, Sánchez Navarro MdC, et al. Green synthesis of silver nanoparticles and their bactericidal and antimycotic activities against oral microbes. *J Nanomater* 2016;2016.
 54. Rashmi B, Harlapur SF, Avinash B, Ravikumar C, Nagaswarupa H, Kumar MA, et al. Facile green synthesis of silver oxide nanoparticles and their electrochemical, photocatalytic and biological studies. *Inorg. Chem Commun*. 2020;111:107580.
 55. Manikandan V, Velmurugan P, Park J-H, Chang W-S, Park Y-J, Jayanthi P, et al. Green synthesis of silver oxide nanoparticles and its antibacterial activity against dental pathogens. *3 Biotech*. 2017;7(1):72.
 56. Tabrizi MH. Fabrication of folic acid-conjugated chitosan-coated PLGA nanoparticles for targeted delivery of Peganum harmala smoke extract to breast cancer cells. *Nanotechnol*. 2022;33(49):495101.
 57. Naiel B, Fawzy M, Halmy MWA, Mahmoud AED. Green synthesis of zinc oxide nanoparticles using Sea Lavender (*Limonium pruinsum* L. Chaz.) extract: characterization, evaluation of anti-skin cancer, antimicrobial and antioxidant potentials. *Sci Rep*. 2022;12(1):1-12.
 58. Singh J, Dutta T, Kim K-H, Rawat M, Samddar P, Kumar P. 'Green'synthesis of metals and their oxide nanoparticles: applications for environmental remediation. *J Nanobiotechnology*. 2018;16(1):1-24.
 59. Kathiraven T, Sundaramanickam A, Shanmugam N, Balasubramanian T. Green synthesis of silver nanoparticles using marine algae *Caulerpa racemosa* and their antibacterial activity against some human pathogens. *Appl*

- Nanosci. 2015;5(4):499-504.
60. Shahryari F, Rabiei Z, Sadighian S. Antibacterial activity of synthesized silver nanoparticles by sumac aqueous extract and silver-chitosan nanocomposite against *Pseudomonas syringae* pv. *syringae*. J. Plant Pathol. 2020;102(2):469-475.
61. El-Belely EF, Farag M, Said HA, Amin AS, Azab E, Gobouri AA, et al. Green synthesis of zinc oxide nanoparticles (ZnO-NPs) using *Arthrospira platensis* (Class: Cyanophyceae) and evaluation of their biomedical activities. Nanomater. 2021;11(1):95.
62. Mourdikoudis S, Pallares RM, Thanh NT. Characterization techniques for nanoparticles: comparison and complementarity upon studying nanoparticle properties. Nanoscale. 2018;10(27):12871-934.
63. Movagharnia R, Baghbani-Arani F, Sadat Shandiz SA. Cytotoxicity effects of green synthesized silver nanoparticles on human colon cancer (HT29) cells. J Kashan Univ Med Sci--Fez. 2018;22(1):31-38.
64. Ghandehari S, Homayouni Homayouni Tabrizi M, Ardalan P. Study of antioxidant properties and toxicity of silver nanoparticles synthesized by aqueous extract of *Rubia tinctorum* on liver cancer cells (HepG2) compared to normal HDF cells. JIUMS. 2018;26(2):57-67.
65. Patnaik S, Berehu HM, Khan I, Chakraborty R, Lavudi K, Mohapatra B, et al. Cytotoxic Potential of Biogenic Zinc Oxide Nanoparticles Synthesized From *Swertia chirayita* Leaf Extract on Colorectal Cancer Cells. Front Bioeng Biotechnol. 2021:1276.
66. Lee S, Jung Y, Oh S, Song E, Choi S, Han H. *Vibrio vulnificus* VvhA induces NF- κ B-dependent mitochondrial cell death via lipid raft-mediated ROS production in intestinal epithelial cells. Cell Death Dis. 2015;6(2):1655.
67. Ahmadi Shadmehri A, Namvar F, Miri H, Yaghmaei P, Nakhaei Moghaddam M. Assessment of antioxidant and antibacterial activities of Zinc Oxide nanoparticles, Graphene and Graphene decorated by Zinc Oxide nanoparticles. Int J Nano Dimens. 2019;10(4):350-358.
68. Moteriya P, Padalia H, Chanda S. Characterization, synergistic antibacterial and free radical scavenging efficacy of silver nanoparticles synthesized using *Cassia roxburghii* leaf extract. J Genet Eng Biotechnol. 2017;15(2):505-513.
69. Moteriya P, Chanda S. Synthesis and characterization of silver nanoparticles using *Caesalpinia pulcherrima* flower extract and assessment of their *in vitro* antimicrobial, antioxidant, cytotoxic, and genotoxic activities. Artif. Cells Nanomed. Biotechnol. 2017;45(8):1556-1567.
70. Bin-Jumah M, Monera A-A, Albasher G, Alarifi S. Effects of green silver nanoparticles on apoptosis and oxidative stress in normal and cancerous human hepatic cells *in vitro*. Int J Nanomedicine. 2020;15:1537.
71. Lee SH, Pie J-E, Kim Y-R, Lee HR, Son SW, Kim M-K. Effects of zinc oxide nanoparticles on gene expression profile in human keratinocytes. Mol Cell Toxicol. 2012;8(2):113-118.
72. Bai D-P, Zhang X-F, Zhang G-L, Huang Y-F, Gurunathan S. Zinc oxide nanoparticles induce apoptosis and autophagy in human ovarian cancer cells. Int J Nanomedicine. 2017;12:6521.
73. Gurunathan S, Lee K-J, Kalishwaralal K, Sheikpranbabu S, Vaidyanathan R, Eom SH. Antiangiogenic properties of silver nanoparticles. Biomater. 2009;30(31):6341-6350.
74. Yang T, Yao Q, Cao F, Liu Q, Liu B, Wang X-H. Silver nanoparticles inhibit the function of hypoxia-inducible factor-1 and target genes: Insight into the cytotoxicity and antiangiogenesis. Int J Nanomedicine. 2016;11:6679.
75. Sheikpranbabu S, Kalishwaralal K, Venkataraman D, Eom SH, Park J, Gurunathan S. Silver nanoparticles inhibit VEGF-and IL-1 β -induced vascular permeability via Src dependent pathway in porcine retinal endothelial cells. J Nanobiotechnology. 2009;7(1):1-12.
76. Tada-Oikawa S, Ichihara G, Suzuki Y, Izuoka K, Wu W, Yamada Y, et al. Zn (II) released from zinc oxide nano/micro particles suppresses vasculogenesis in human endothelial colony-forming cells. Toxicol Rep. 2015;2:692-701.